J Mater Sci (2008) 43:621–634
DOI 10.1007/s10853-007-2170-0

Protonated niobate/titanate pyrochlores via lead-acid exchange in $Pb_{1.5}Nb_2O_{6.5}$ and $Pb_2Nb_{1.33}Ti_{0.67}O_{6.67}$

Alicia B. Brune · Robert I. Mangham · William T. Petuskey

Received: 16 January 2007 / Accepted: 14 September 2007 / Published online: 17 October 2007

Abstract Hydrogen-based niobates and niobate-titanates were derived from the pyrochlores $Pb_{1.5}Nb_2O_{6.5}$ (PN) and $Pb_2Nb_{1.33}Ti_{0.67}O_{6.67}$ (PNT) by ion exchange in acid baths, affording sub-micron size white powders. The niobium sublattice was left intact, as shown by X-ray diffraction. A combination of stripping and thermogravimetric analyses gave the effective formulas $H_{2.66}Pb_{0.17}Nb_2O_{6.5}\cdot 0.5H_2O$ (HPN) and $H_{3.88}Pb_{0.06}Nb_{1.33}Ti_{0.67}O_{6.67}\cdot 0.33H_2O$ (HPNT). The corresponding structural refinements gave good fits to the XRD data. Densities measured by He pycnometry agreed with densities calculated from XRD analyses and the effective formulas. Thermal stability was assessed by TGA, DSC, and XRD. With increasing temperature, HPN and HPNT lost weight (H_2O), becoming amorphous, and then transforming to crystalline phases, with greatly reduced particle size. HPN was more stable than HPNT. The electrical conductivities of powder compacts in wet atmospheres were moderate and attributed mainly to proton conduction; i.e., 10^{-6} to 10^{-5} S cm^{-1} for HPN and 10^{-7} to 10^{-6} S cm^{-1} for HPNT (from room temperature to 230 °C). Experimental results were interpreted in terms of Nb(V) being a stronger electron acceptor than Ti(IV).

Introduction

This article describes the preparation and characterization of hydrogenated pyrochlores (abbreviated as HPN and HPNT) obtained from $Pb_{1.5}Nb_2O_{6.5}$ (PN) and $Pb_2Nb_{1.33}Ti_{0.67}O_{6.67}$ (PNT), respectively, by ion exchange in acidic aqueous media. Characterization of crystalline structures was done by X-ray powder diffraction. The structural data, in conjunction with thermal analysis, electrochemical stripping analysis, and helium pycnometry results, were applied to evaluate the effective formulas for HPN and HPNT. Their thermal stabilities and electrical conductivities were assessed.

Both of the parent compounds have the pyrochlore structure [1]. The tendency to exchange the larger and more labile cations, while preserving the original crystallographic structure, has been reported for several pyrochlores, e.g. [2–10], but not for PN and PNT themselves. In particular, hydrated niobium oxides with the pyrochlore structure were prepared by exchanging Tl(I) [2] or Ca(II) [8] cations in the respective niobates. The pyrochlore type structure is adopted by oxides of general formula $A_2B_2O_7$, where cation A is relatively large and cation B has a high oxidation state [11–15]. The lattice is cubic (distorted), with space group Fd-3m, and consisting of eight effective formulas per unit cell [16]. Consistent with most literature reports (e.g. [15]), we have adopted the origin B_o (0,0,0). Site symmetries are: B in 16c, A in 16d, (6/7) O in 48f, and (1/7) O (represented by Ó) in 8b crystallographic positions. A positional parameter x for the 48f O site [16], accounts for distortions. This structure can be viewed as an infinite network of corner sharing BO_6 octahedra that form cages filled with A and Ó ions. The stoichiometry of pyrochlores can deviate from the ideal $A_2B_2O_7$ [17], resulting in a deficiency in the A, B, and Ó sites occupancies. PN and PNT are both non-stoichiometric, corresponding to the general formulas $Pb_{1.5\square}Nb_2O_{6.5\square}$ and $Pb_2(Nb_{1.33}Ti_{0.67})_\square O_{6.67\square}$. Here, □ refers to vacancies.

When the A cations in a pyrochlore are exchanged in acidic aqueous media, hydrogen containing species enter the lattice to maintain charge balance and stabilize the

A. B. Brune (✉) · R. I. Mangham · W. T. Petuskey
Department of Chemistry and Biochemistry, Arizona State University, 871604, Tempe, AZ, USA
e-mail: alicia.brune@asu.edu

structure. Considerable work has been devoted to establish the exact nature and location of these species: Hydronium ions and hydration water that fill intra-molecular cavities, and –OH groups taking the place of framework oxygens—one or more of them—have been reported [2–4, 7–9, 18–24]. Surface bound and inter-crystalline water can also be present. High proton conductivity has been observed in the exchanged compounds, e.g. [3–5, 7, 25, 26]. This suggests HPN and HPNT could also be suitable for proton conducting membranes. Some other possible applications would be as precursors in inorganic synthesis, as highly specific ion exchangers [10], and in catalysis [27], photocatalysis [28], and the sequestration and storage of small gas molecules.

Experimental

Reagents

The following reagents and their sources were used in our syntheses: niobium pentoxide Nb_2O_5 (Aldrich Chemical Co. 99.9% metal basis, <325 mesh); titanium oxide TiO_2, with rutile phase (Aldrich Chemical Co. 99.9% metal basis, <325 mesh); orthorhombic lead oxide PbO (Alfa Aesar 99.99%); concentrated HNO_3 and HCl, 30% (v/v) H_2O_2 (various vendors); He, O_2, and N_2 (max. H_2O 1.5 ppm).

Synthesis of HPN and HPNT

The synthesis of $Pb_3Nb_4O_{13}$ [1, 29, 30] started with the stoichiometric combination of PbO and Nb_2O_5 (both were dried at 120 °C, prior to weighing and mixing). They were ground and thoroughly mixed in an agate mortar, packed in MgO crucibles, heated first to 800 °C in air for 2 h, to 1,000 °C for about 15 h, and then furnace cooled. Powders were re-ground, formed into pellets, and annealed at 1,150 °C for 10 h to complete the solid state reaction and homogenization. Crystallinity and phase purity of the resulting lead niobiate were confirmed by X-ray diffraction.

In second step, the lead niobate was treated in an acid wash for several hours between 70 and 80 °C, with magnetic stirring. The wash consisted of one part water and one part acid mix solution made of three parts of HNO_3 and one part of HCl, both concentrated. Afterwards, the solids were settled out from the wash by centrifugation. Supernatants were discarded and the solids were washed and centrifuged several more times with distilled water. The white powders, thus obtained, were dried at room temperature, 85 or 130 °C, depending on the experiment to be performed.

The same procedure was followed for powders of the Nb–Ti series. In this case, the starting oxides were PbO, Nb_2O_5 and TiO_2. Ion exchange was done with the acid wash between 80 °C–90 °C, for 48 h. The resulting white HPNT powders were washed and dried at 85 °C.

Characterization methods

The heavier elements, Nb, Ti, and Pb, were detected by electron probe micro-analysis. All constituting elements were evaluated by Ion Beam Analysis. Quantitative analysis of residual lead was done by anodic stripping voltammetry. The microstructure was observed by scanning electron microscopy. Phase composition and crystallographic structures were investigated by X-ray powder diffraction. Structural refinements were carried out by a Rietveld least squares method. Thermal analysis established thermal stability limits, and complemented the stripping analysis data for determining the effective formulas. Density, measured by pycnometry, was compared with the density calculated from the formula weight and the unit cell volume, as determined by X-ray diffraction. Electrical conductivity was measured by AC techniques. Solubility in peroxide solutions, previously reported in related compounds [31], was assessed with the objective of preparing samples for stripping analysis.

Instrumentation and measurements

Images of the synthesized powders were taken using JEOL JSM T200, JEOL SEM 480, and a Hitachi 4700-II FE-SEM scanning electron microscopes. The heavier elements in HPN and HPNT were detected by wavelength dispersive X-ray spectroscopy, using an electron probe micro-analytical system JEOL JXA 8600 [1]. All elements were evaluated by Ion Beam Analysis (IBA) equipped with a General Ionex accelerator IBA. Oxygen was detected by Rutherford Backscattering (RBS), hydrogen by Electron Recoil Detection (ERD), and the heavier elements by Proton Induced X-ray Emission (PIXE).

Quantitative analysis of the small amounts of lead, remaining in HPN and HPNT after cation exchange, was accomplished by anodic stripping voltammetry, combined with sequential additions of a lead standard for calibration. With this method the oxides were dissolved (digested) in acid solutions. The dissolved lead was electrochemically accumulated onto a glassy carbon electrode, as a mercury amalgam, and then electrochemically stripped. The stripping peak currents and integrated peak areas were proportional to the amount of lead in solution. Details of the stripping method and equipment are given in the

Appendix. The method is precise and sensitive to nanomolar concentrations of the analyte.

X-ray diffraction patterns were obtained using a Siemens D5000 diffractometer [1], with Cu $K\alpha_1$ radiation, wavelength 1.540562 Å. The diffraction data were displayed and processed with software programs EVA 5.0 and Materials Data Jade 8.2. Rietveld analysis of the X-ray powder diffraction data was done with GSAS software, developed by Larson and von Dreele [32]. ICDD cards were accessed with the software package PD4+ 2005. Thermogravimetric analysis (TGA), between room temperature and 800 °C, was carried out using mostly Perkin Elmer Pyris 1 TGA, in Pt crucibles without a lid, under flowing O_2, N_2, or He (flow rate 50 mL/min). Differential scanning calorimetry (DSC) and simultaneous thermogravimetric analysis (TGA) were done from room temperature up to 600 °C in a Netzsch Instruments Jupiter STA 449 C, using alumina crucibles with and without perforated lids, under flowing O_2 (flow rate 50 mL/min). Low temperature DSC was done using a TA (Thermo-Analytical) calorimeter, in sealed aluminum capsules.

The density of the powders, compressed into pellets of known mass, was determined by helium displacement pycnometry (Micromeritics AccuPyc 1330). AC electrical conductivity measurements were performed using a programmable, automatic RCL meter Philips PM 6304, under controlled temperature in dry and wet atmospheres. The wet atmosphere was established by passing nitrogen first through a water bubbler at room temperature and then through the sample chamber, which was in a controlled temperature oven. A dry atmosphere was established in the conductivity chamber before introducing water vapor. Conductivity samples were in the form of cylindrical pellets (cold pressed, diameter ~0.7 cm, height ~0.2 cm). Contacts were made with silver paint, silver foil and silver leads.

Results

Microstructure

The SEM micrograph of HPN in Fig. 1 depicts a material with aggregates of fine powders, of sub-micron particle size. HPNT presented similar microstructures.

Elemental composition

The elements Pb and Nb in HPN, and Pb, Nb, and Ti in HPNT, were detected by electron probe micro-analysis. Ion beam analysis showed that HPN contained Nb, O, H, and small amounts of lead. Instability and chemical complexity

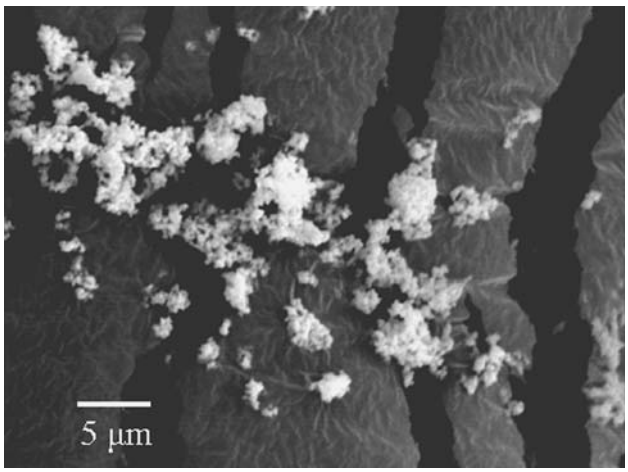

Fig. 1 Scan electron micrograph (in secondary emission mode) of HPN powders dried at 130 °C

of the samples precluded the use of electron and ion beam techniques for quantitative determinations of lead. Instead, an electrochemical stripping analysis procedure, with sequential additions for calibration, was developed and applied to determine the residual lead (see Appendix). Graphs of stripped lead (expressed as charge) versus spiked lead concentration, in solutions of HPN (HPNT), are shown in Fig. 2(a) (HPN) and (b) (HPNT). As described in the Appendix, extrapolations to zero charge gave the amounts of lead already in the solutions, and thereby in the powders. Lead concentrations in solution (mean values with their standard deviations) were 1.99 ± 0.09 µM (HPN), and 0.943 ± 0.046 µM (HPNT). The corresponding weight percentages of residual lead in HPN and HPNT powders were determined, knowing the volume in the stripping cell (10 mL) to which 15 µL had been added, of solutions with 260 mg HPN /100 mL and 300 mg HPNT/100 mL, respectively. The weights were 10.6% for HPN and 4.34% for HPNT. The atom % composition of HPN, evaluated by ion beam analysis, was H 14%, Pb 1%, Nb 21%, and O 64%, with maximum error 2%.

X-ray diffraction patterns and TGA and DSC profiles

X-ray powder diffraction patterns of the dried materials, before and after acid exchange, are shown in Fig. 3(a) (PN), Fig. 3(b) (HPN), Fig. 4(a) (PNT), and Fig. 4(b) (HPNT).

TGA traces of HPN heated to 600 °C at 5 °C/min under flowing oxygen are shown in Fig. 5. Prior to thermal analysis, the sample in Fig. 5(a) was dried at 130 °C in air and the sample for Fig. 5(b) was dried at room temperature, again in air. Most, if not all weight loss occurred below 240 °C. A total weight loss of 10% was observed in

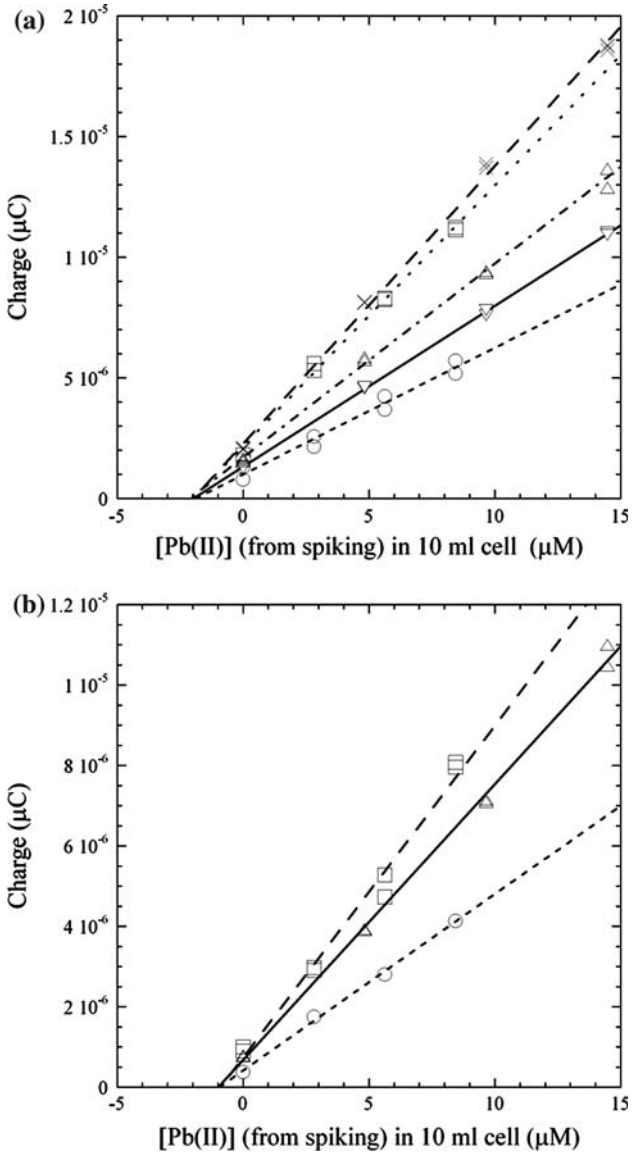

Fig. 2 Graphs showing stripped lead (expressed as charge) versus lead concentration due to "spiking" (see Appendix), in solutions containing known amounts of dissolved HPN (**a**) and HPNT (**b**)

samples dried at 130 and 85 °C (not shown). This was twice as much for the sample dried at room temperature. No weight was re-gained upon cooling, for all samples heated to 600 °C. The X-ray diffraction pattern, taken after thermal analysis, did not resemble that of HPN, but a polymorph of Nb_2O_5 (ICDD 00-028-0317).

For HPN samples heated to only 240 °C, some weight was re-gained upon cooling. Their X-ray patterns, after TGA, showed strong amorphous backgrounds, with superimposed peaks of low intensity at reflection angles indicative of residual crystalline HPN (Fig. 6). HPN samples heated to 170 °C for 2 h, recovered practically all weight losses upon cooling, regardless of whether they were exposed to flowing helium (Fig. 7(a)), oxygen (Figs. 7(b) and (c)), or nitrogen (Fig. 7(d)). No significant changes in the X-ray pattern were detected.

Combined DSC and TGA were applied to HPN samples under flowing oxygen (Fig. 8). The TGA profile indicated two different weight loss processes characterized by two different weight/temperature slopes. The second process corresponded with an endothermic reaction in the DSC profile (peak at 295 °C). The DSC profiles also showed an exothermic reaction at higher temperatures (peak at 540 °C), with no weight change (TGA). Enthalpy changes, relative to the initial weight of HPN, were 41.6 J/g for the endothermic reaction at 295 °C, and –37.4 J/g for the exothermic at 540 °C. The data in Fig. 8 were taken using a crucible without lid. When using a crucible with a perforated lid, TGA and DSC profiles shifted to higher temperatures. Evidently, the gas atmosphere generated within the capsules hindered thermal decomposition. No thermal events were seen in DSC of HPN, cooled from room temperature to –100 °C.

Samples of HPNT, initially dried at 85 °C, exhibited maximum weight losses of 15% when heated to 600 or 800 °C, at 5 °C/min under flowing oxygen or nitrogen. After TGA to 800 °C, the XRD pattern was approximately that of a niobium–titanium oxide (ICDD 01-070-2009). Unlike HPN, HPNT samples heated to 170 °C by TGA in oxygen or nitrogen (Fig. 9), showed practically no weight recovery after cooling and their XRD patterns corresponded to a mostly amorphous material. A dark color developed in TGA samples heated to 240 °C. DSC of HPNT, cooled from room temperature to –100 °C, did not show any thermal events.

The crystallite particle size, estimated by applying the Scherrer equation to XRD data (through JADE software), was 117 nm in HPN dried at 130 °C (Fig. 3(b)), 8 nm in crystalline HPN mixed with mostly amorphous material (Fig. 6) and 17 nm in the crystalline niobium oxide that resulted from heating HPN to 600 °C.

Evaluation of the effective formulas

In evaluating the formulas, we considered two cases:

Case I. If it is assumed that two H^+ cations replaced each Pb^{2+} cation exchanged, while the pyrochlore skeleton remained unchanged, the formulas of the exchanged pyrochlores could then be written as $H_{2x}Pb_{(1.5-x)}Nb_2O_{6.5}$ (HPN) and $H_{2x}Pb_{(2-x)}Nb_{1.33}Ti_{0.67}O_{6.67}$ (HPNT). Assuming that, during the exchange, water molecules fill the oxygen vacancies sites (Ó vacancies in 1/2 of 8b sites) in the defective pyrochlores, those formulas would become $H_{2x}Pb_{(1.5-x)}$ $Nb_2O_{6.5}{\cdot}0.5H_2O$ (HPN) and $H_{2x}Pb_{(2-x)}Nb_{1.33}Ti_{0.67}O_{6.67}{\cdot}0.33H_2O$ (HPNT). With these assumptions and the lead weight percentage values measured by stripping analysis, the effective formulas,

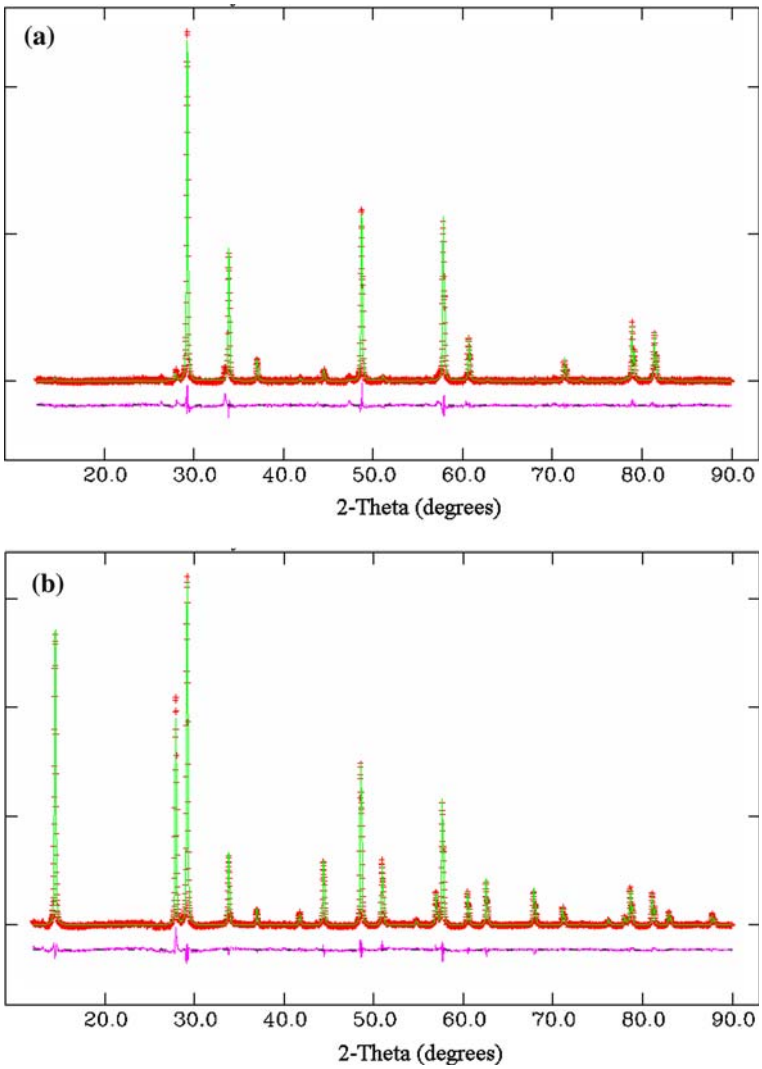

Fig. 3 Experimental (+) and calculated (–) XRD patterns of (**a**) PN and (**b**) HPN (dried at 130 °C); XRD at room temperature, step size 0.017 degrees. *Reduced* $\chi^2 = 2.79$ (**a**) and 3.96 (**b**); *wRp%* = 7.15 (**a**) and 4.06 (**b**)

residual lead occupancies, and maximum possible water losses evaluated are shown in Table 1 (case I), together with the weight losses measured by TGA to 600 °C.

Case II. If it is assumed that two hydronium (H_3O^+) cations replaced each Pb^{2+} cation exchanged, the formulas of the exchanged products would be $(H_3O)_{2x}Pb_{(1.5-x)}Nb_2O_{6.5}$ (HPN) and $(H_3O)_{2x}Pb_{(2-x)}Nb_{1.33}Ti_{0.67}O_{6.67}$ (HPNT). Based on these assumptions and the lead weight percentage values measured by stripping analysis, the effective formulas, residual lead occupancies and maximum possible water losses evaluated are shown in Table 1 (case II). With these formulas, maximum water losses were significantly higher than the weight losses measured by TGA; no extra water in oxygen vacancy sites was considered.

The effective formulas derived under the assumptions in cases (I) and (II), and possible intermediate cases, are discussed and discriminated in the discussion section, taking into account the literature results [2–4, 7–9, 18–24] on hydrogen-based pyrochlores.

The effective formula for HPN, derived from ion beam analysis data, was $H_{1.33}Pb_{0.1}Nb_2O_{6.10}$. This had relatively less hydrogen, oxygen, and lead than the effective formulas derived from stripping and thermal analyses. The discrepancy is attributed to sample interactions with the ion beam.

Structural refinements

Rietveld refinements of structural models, to fit HPN and HPNT X-ray diffraction data, were based on the pyrochlore structure [11–15], the structural data reported for the parent compounds (PN in [33] and ICDD 01-084-1731, PNT in ICDD 04-002-2975), and the experimentally determined stoichiometries (Table 1, case I). Calculated X-ray patterns are shown in Fig. 3(b) (HPN) and 4(b) (HPNT), and

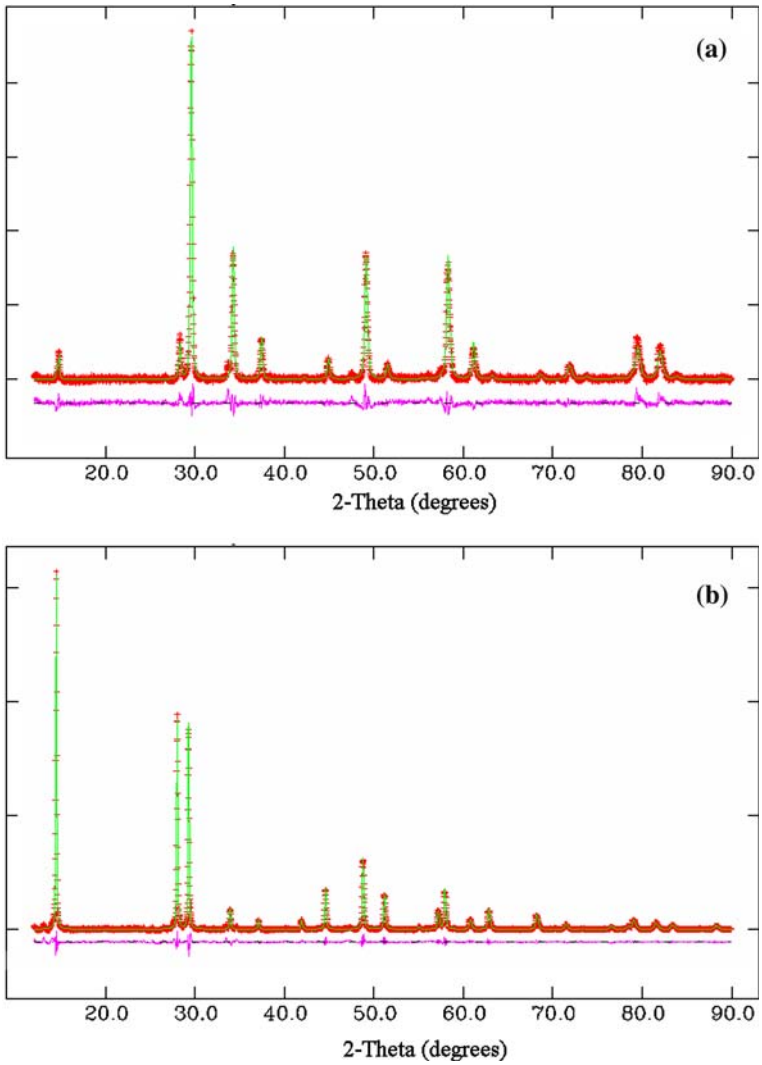

Fig. 4 Experimental (+) and calculated (–) XRD patterns of (**a**) PNT and (**b**) HPNT (dried at 85 °C); XRD at room temperature, step size 0.017 degrees. *Reduced* χ^2 = 2.44 (**a**) and 3.46 (**b**); *wRp%* = 8.73 (**a**) and 5.86 (**b**)

compared to the experimental data. The refined unit cell lattice parameters were 10.605 Å (HPN) and 10.559 Å (HPNT). Atomic coordinates and site occupancies are given in Tables 2 (HPN) and 3 (HPNT). The goodness of fit parameters *Reduced* χ^2 and *wRp* [32] are shown with the figures legends. Case I formulas, but without water molecules in oxygen vacancies sites (1/2 of 8 b sites), were tested. They yielded higher computational residuals, in agreement with results reported in [8]. It was not possible to achieve a good fit to the XRD data by assuming all the lead had been removed by ion exchange.

In addition to refining the structural models for HPN and HPNT, it was confirmed that the models reported in the literature for the parent pyrochlores (PN and PNT) did fit the XRD patterns of the powders from which HPN and HPNT were made, respectively. The continuous lines in Figs. 3(a) (PN) and 4(a) (PNT) show the calculated patterns, superimposed to the observed ones. Lattice parameters (PN: a = 10.5647 Å, PNT: a = 10.515 Å), atomic coordinates and sites occupancies, were taken from the literature (PN: [33] and ICDD 01-084-1731; PNT: ICDD 04-002-2975), with the exception of the x coordinate for PNT, refined to 0.303. The goodness of fit parameters are shown with the figures legends.

Refined peak positions and relative intensities are given in Tables 4 (HPN) and 5 (HPNT). In addition to HPN and HPNT, no other phases were detected by XRD. For comparison, peak positions and intensities for PN and PNT, consistent with the pyrochlore structure, are also shown in Tables 4 and 5.

He pycnometry

HPN and HPNT densities and their standard deviations were measured by helium displacement pycnometry at room temperature. They are listed in Table 6, together with the densities evaluated from the effective formulas for case

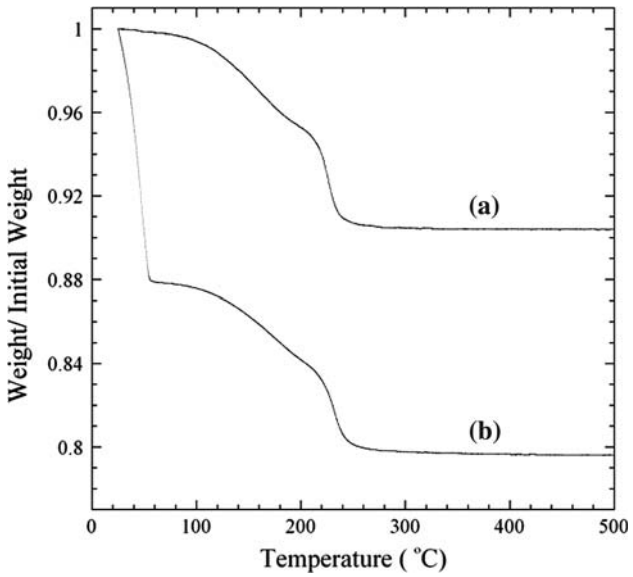

Fig. 5 TGA to 600 °C of HPN dried at 130 °C (**a**) and room temperature (**b**). Sample weight in (**a**): 7.62 mg and (**b**): 14.55 mg. Scan rate 5 °C/min; oxygen atmosphere; Perkin Elmer instrument

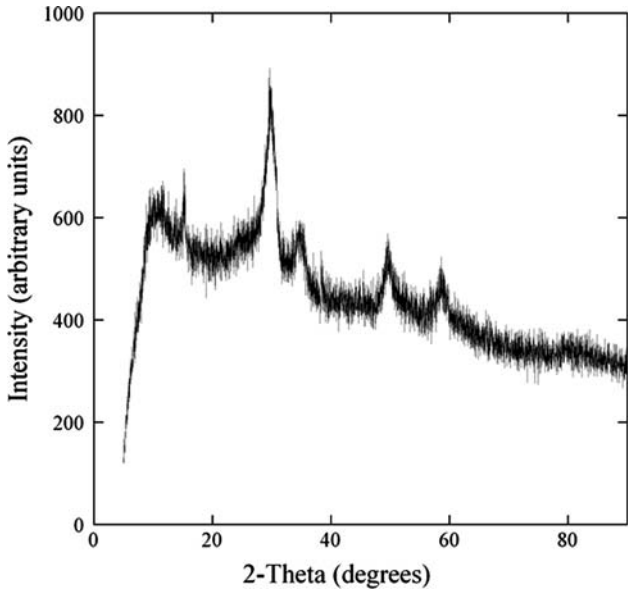

Fig. 6 XRD pattern of HPN powders, taken at room temperature with step size 0.017 degrees, after TGA to 240 °C in oxygen atmosphere, Perkin Elmer instrument

I and the lattice parameters. Also shown are HPN and HPNT molar volumes.

AC conductivity

Impedance measurements, in a wet atmosphere, were taken at frequencies from 50 Hz to 100 KHz, between 293 and 500 K. The wet atmosphere was achieved by introducing

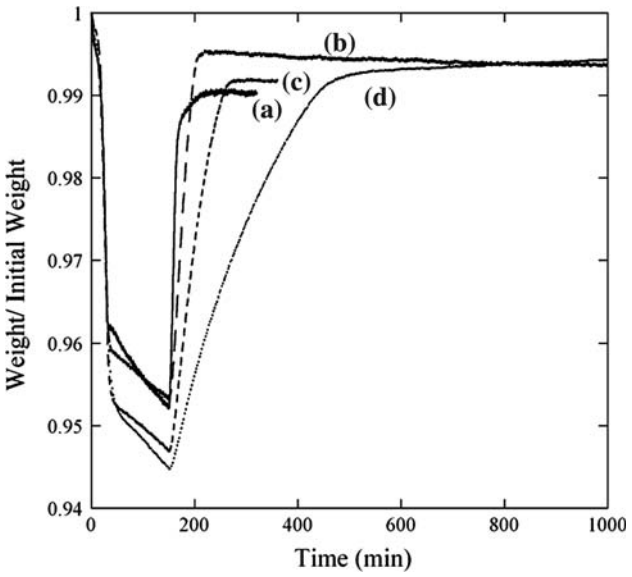

Fig. 7 TGA to 170 °C of HPN samples dried at 130 °C. Thermal program: heating to 170 °C at 5 °C /min, held 120 min at 170 °C, and cooling to room temperature. Atmospheres were (**a**) helium, (**b**) and (**c**) oxygen and (**d**): nitrogen. Sample weight (**a**) 6.28 mg, (**b**) 7.84 mg, (**c**) 10.40 mg, and (**d**) 14.88 mg; Perkin Elmer instrument

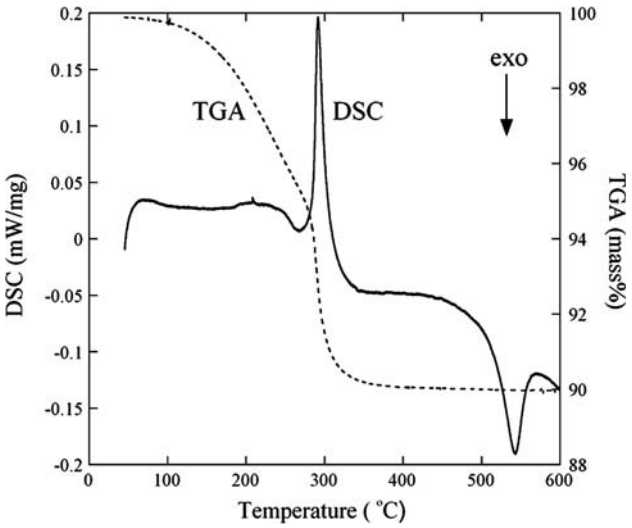

Fig. 8 DSC and TGA to 500 °C of HPN dried at 130 °C. Sample weight: 42.17 mg; scan rate 5 °C/min; oxygen atmosphere; Netzsch instrument

water vapor into the conductivity chamber, as described in the experimental section. Nyqst plots exhibited predominantly single, depressed arcs. The electrical conductivity was derived from the resistance measured at the right intercept of each impedance arc with the real axis, according to the procedures outlined in the literature [34].

HPN conductivity was in the range of 10^{-6} to 10^{-5} S cm^{-1}. An Arrhenius plot is shown in Fig. 10 together with literature data for a related compound [9]. In both cases the conductivity went through a minimum with

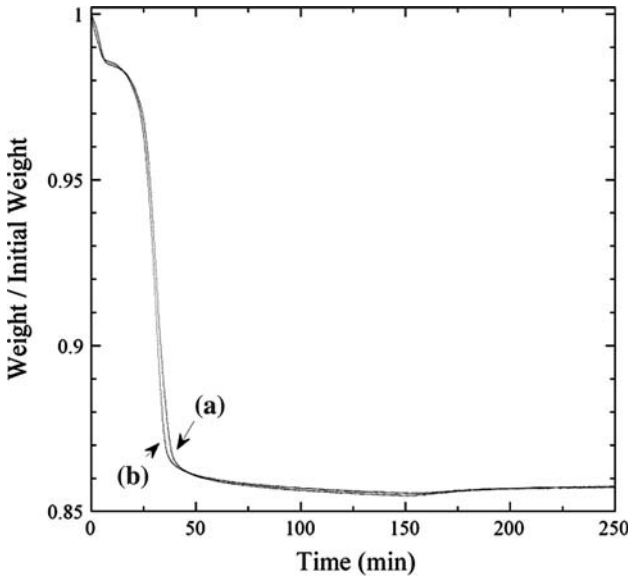

Fig. 9 TGA of a HPNT sample dried at 85 °C; program and equipment were the same as in Fig. 7. Atmosphere: (**a**) oxygen and (**b**) nitrogen; sample weight (**a**) 17.59 mg and (**b**) 13.21 mg

increasing temperatures. The activation energy, estimated at the higher temperatures, was 0.2 eV. The conductivity decreased with thermal cycling. At room temperature, the electrical conductivity of HPN (dried at 130 °C) increased when switching from dry to wet atmospheres, as shown in Fig. 11. HPNT was less conductive in wet atmospheres (10^{-7} to 10^{-6} S cm^{-1}) than HPN, and its conductivity was less responsive to the presence of moisture.

Solubility

HPN and HPNT samples needed to be dissolved, to perform stripping analysis. To test their solubility as peroxo complexes, small amounts of HPN (HPNT) powders were weighed out and added to test tubes containing a few milliliters of H_2O_2 aqueous solutions, acidified with HNO_3 and kept at 60–70 °C. In a few hours, the powders dissolve. Solubility exceeded 2.5 mg/mL. The solutions turned color after dissolving the solids, i.e. to yellow in the case of HPN and orange for HPNT. The solutions remained stable for more than a year.

Table 2 Atomic parameters in GSAS refinement for HPN

Atom	Position	Coordinates *x y z*	Occupancy
Pb	16d	0.5 0.5 0.5	0.085
Nb	16c	0 0 0	1
O(I)	8b	0.375 0.375 0.375	1
O(II)	48f	0.312 0.125 0.125	1

Table 3 Atomic parameters in GSAS refinement for HPNT

Atom	Position	Coordinates *x y z*	Occupancy
Pb	16d	0.5 0.5 0.5	0.03
Nb	16c	0 0 0	0.67
Ti	16c	0 0 0	0.33
O(I)	8b	0.375 0.375 0.375	1
O(II)	48f	0.314 0.125 0.125	1

Discussion

The determination of residual lead in HPN and HPNT powders provided the basis for the evaluation of their effective chemical formulas. The formulas were derived under two different assumptions: Pb^{2+} exchanged for H^+ (case I, Table 1) or Pb^{2+} exchanged for H_3O^+ (case II, Table 1). Only the formulas in case I are consistent with the experimental data. Weight losses calculated from these formulas were in agreement with those measured by TGA (Table 1). Moreover, the formulas in case I led to successful Rietveld refinements. Densities, calculated from the corresponding formula weights and refined lattice parameters, agreed with experimental density values (Table 6).

Most recent studies on the nature and location of hydrogen containing species in acid exchanged pyrochlores used neutron diffraction methods. In some cases, they concluded that H_3O^+ in 8a channels were the dominant species [24], while a combination of H_2O, –OH, and H_3O^+ prevailed in others [23]. Regarding HPN and HPNT, we did not find evidence of H_3O^+. A very small contribution of H_3O^+ to the proposed formulas in case I may explain the minor differences in weight loss between the theoretical and the experimental values (Table 1), although we think that residual surface and inter-crystalline water provide an equally viable argument.

Table 1 Effective formulas, calculated lead occupancies and water losses, and TGA weight losses for HPN and HPNT

	Effective formula	Lead occupancy %	Calculated maximum water loss %	TGA weight loss %
Case I	$H_{2.66}Pb_{0.17}Nb_2O_{6.5}\cdot 0.5H_2O$	8.5	9.8	10
	$H_{3.88}Pb_{0.06}Nb_{1.33}Ti_{0.67}O_{6.67}\cdot 0.33H_2O$	3	14.4	15
Case II	$(H_3O)_{2.62}Pb_{0.19}Nb_2O_{6.5}$	9.5	18.6	10
	$(H_3O)_{3.85}Pb_{0.07}Nb_{1.33}Ti_{0.67}O_{6.67}$	3.5	29.8	15

Table 4 X-ray diffraction data for PN and HPN

$Pb_{1.5}Nb_2O_{6.5}$ICDD 01-084-1731				HPN (GSAS refinement)		
2θ	d (Å)	I (‰)	*h k l*	2θ	d (Å)	I (%)
14.510	6.0995	6	111	14.455	6.1227	87.0107
23.802	3.7352	2	220	23.711	3.7493	3.5491
27.988	3.1854	20	311	27.880	3.1974	65.8270
29.259	3.0498	999	222	29.147	3.0613	100
33.913	2.6412	337	400	33.781	2.6512	26.5310
37.061	2.4237	40	331	36.916	2.4329	6.7076
41.855	2.1565	8	422	41.690	2.1647	4.2057
44.526	2.0332	21	511	44.349	2.0409	4.9538
			333	44.349	2.0409	15.7950
48.717	1.8676	332	440	48.522	1.8747	53.6932
51.106	1.7858	6	531	50.900	1.7925	24.7696
51.885	1.7608	1	442	51.674	1.7674	0.0000
54.920	1.6704	2	620	54.695	1.6767	2.6579
57.124	1.6111	2	533	56.889	1.6172	12.0596
57.846	1.5927	302	622	57.608	1.5987	45.3039
60.681	1.5249	82	444	60.429	1.5306	10.7605
62.757	1.4794	2	711	62.493	1.4849	5.3430
			551	62.493	1.4849	10.6321
66.133	1.4118	1	642	65.852	1.4171	0.0105
			552	67.825	1.3806	2.5194
68.117	1.3754	3	731	67.825	1.3806	11.5626
71.364	1.3206	37	800	71.054	1.3256	8.1034
73.282	1.2907	3	733	72.961	1.2955	0.9296
73.917	1.2812	1	644	73.592	1.2860	0.0000
			660	76.098	1.2498	0.7762
76.438	1.2451	2	822	76.098	1.2498	1.3224
78.310	1.2199	4	751	77.959	1.2245	2.7294
			555	77.959	1.2245	0.1220
78.932	1.2119	89	662	78.577	1.2164	14.2919
81.405	1.1812	79	840	81.034	1.1856	11.8517
			753	82.866	1.1640	3.1543
83.249	1.1596	2	911	82.866	1.1640	2.1638
83.863	1.1527	1	842	83.475		
86.308	1.1262	1	664	85.904	1.1304	0.8844
88.138	1.1075	1	931	87.721	1.1169	5.2336

2θ, Bragg angles; d, lattice spacings; I, relative intensities; *h k l*, Miller indices

In agreement with the behavior observed in other pyrochlores [2–10], PN and PNT exchanged their bulkier, most weakly bound cations, after several hours in acid baths. The exchange did not run to completion for either compound, as determined by stripping analysis for residual lead. The pyrochlore skeleton was essentially preserved (Figs. 3 and 4, Tables 4 and 5), suggesting that the presence of residual lead may have had a role in stabilizing the open framework structure. This does not occur naturally in niobic acids.

Experimental results indicated that weight losses, due to water, were later re-gained by HPN when annealed at 170 °C (Fig. 7). This was practically independent of the carrier gas employed, indicating that residual water was scavenged from the gas. Thermal analysis gave an insight on how dehydration coupled to the collapse of the pyrochlore structure. Several processes could be distinguished. Below about 100 °C, HPN previously dried in air (Fig. 5(b)), rapidly lost water that was originally physisorbed. At higher temperatures, two crystallographic water

Table 5 X-ray diffraction data for PNT and HPNT

$Pb_2Nb_{1.33}Ti_{0.67}O_{6.67}$ ICDD 04-002-2975				HPNT (GSAS refinement)		
2θ	d (Å)	I (‰)	*h k l*	2θ	d (Å)	I (%)
14.579	6.0708	161	111	14.518	6.0962	100
23.916	3.7176	1	220	23.816	3.7331	2.0777
28.123	3.1704	106	311	28.004	3.1836	70.6052
29.401	3.0354	999	222	29.276	3.0481	71.6373
34.078	2.6288	357	400	33.932	2.6397	9.8464
37.243	2.4123	109	331	37.083	2.4224	3.0607
42.062	2.1464	4	422	41.880	2.1553	3.8722
			333	44.552	2.0320	15.4730
44.747	2.0236	51	511	44.552	2.0320	4.2245
48.962	1.8588	328	440	48.746	1.8665	37.0675
51.365	1.7774	37	531	51.137	1.7847	18.7408
			442	51.916	1.7598	0.0385
55.201	1.6626	2	620	54.953	1.6695	1.1365
57.419	1.6035	8	533	57.159	1.6102	11.1304
58.145	1.5852	307	622	57.882	1.5918	24.1655
60.999	1.5177	83	444	60.719	1.5240	6.3621
63.087	1.4724	12	711	62.796	1.4785	4.5728
			551	62.796	1.4785	8.0238
66.486	1.4051	1	642	66.175	1.4110	0.0138
68.483	1.3689	13	731	68.161	1.3746	9.0310
			553	68.161	1.3746	1.5534
71.753	1.3144	37	800	71.410	1.3198	3.8081
73.686	1.2846	8	733	73.330	1.2899	0.3644
			644	73.966	1.2804	0.0059
76.865	1.2392	1	660	76.489	1.2443	0.7847
			822	76.489	1.2443	1.0790
78.752	1.2142	9	751	78.363	1.2192	1.4568
79.379	1.2062	92	662	78.985	1.2111	7.7935
			555	78.363	1.2192	0.0423
81.872	1.1756	79	840	81.461	1.8053	0.2017
83.732	1.1542	8	911	83.307	1.1589	1.7444
			753	83.307	1.1589	1.8898
			842	83.921	1.1520	0.0207
86.817	1.1209	1	664	86.369	1.1255	0.3517
88.664	1.1023	2	931	88.201	1.1068	3.3332

2θ, Bragg angles; d, lattice spacings; I, relative intensities; *h k l*, Miller indices

Table 6 HPN and HPNT densities measured by pycnometry, and the corresponding values calculated from effective formulas and refined lattice parameters

	Density by pycnometry (g/cm^3)	Standard deviation (g/cm^3)	Calculated density (g/cm^3)	Molar volumes (cm^3)
HPN case I	3.8048	0.0161	3.75	89.8
HPNT case I	3.1359	0.0064	3.21	88.7

Also listed are HPN and HPNT molar volumes

loss processes took place. At a scanning rate of 5 °C/min, up to about 170 °C, water was lost with relatively slower rate, indicated by the lower slope in the TGA profiles, Figs. 5 and 8. X-ray diffraction showed no major structural changes. Such water would reside in oxygen sites of the defective pyrochlore [35–37]. Above 170 °C, water was lost at higher rates as indicated by the higher slopes in Figs. 5 and 8. This was concurrent with an endothermic reaction, as detected by a sharp DSC peak centered at 295 °C. It is thought that this reaction involves the

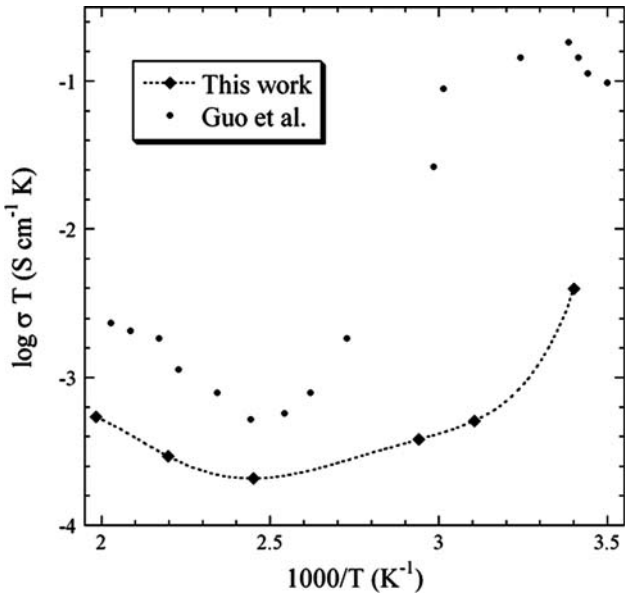

Fig. 10 Arrhenius plot of the electrical conductivity of a compressed HPN powder sample, measured in a wet atmosphere. Literature data from Guo et al. [9] are also shown, reproduced with permission

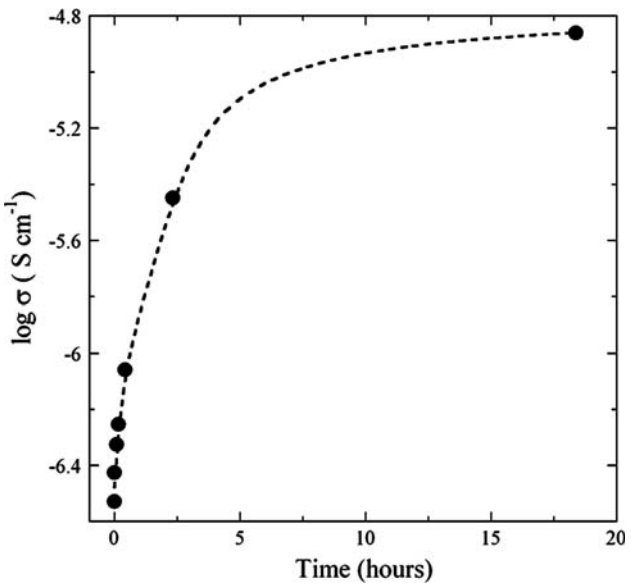

Fig. 11 Logarithm plot of HPN electrical conductivity versus time, in an initially dry atmosphere changed to wet. Measurements were taken at room temperature and 1 KHz

formation of water from hydrogens located near empty Pb-cation sites and from crystallographic hydroxyls. Removal of water produced by this dehydroxylation step resulted in the collapse of the crystalline structure, rendering mostly amorphous material (Fig. 6). Re-crystallization occurred at higher temperatures, around 540 °C, and was exothermic. The enthalpy change for the endothermic dehydroxylation–amorphization at 295 °C was 41.6 J/g (14.0 kJ/mol). This was similar in magnitude to the enthalpy change for re-crystallization at 540 °C, i.e. –37.4 J/g.

HPN had greater tendency to re-gain water than HPNT (Figs. 7 and 9) when cooled to room temperature. This is attributed to greater niobium content for HPN than HPNT. Although the ionic radii of Nb(V) and Ti(IV) are similar, the greater charge for Nb(V) makes it a stronger electron acceptor, more able to retain water.

The electrical conductivity of HPN compressed powders in wet atmospheres was moderate (Fig. 10) and attributed mainly to surface/subsurface proton conduction, similar to what has been proposed for another H-based pyrochlore, $HTaWO_6{\cdot}H_2O$ [18]. Since Nb(V) is a strong electron acceptor, HPN interacts with the water dipoles, releasing protons for conduction. The impedance spectra were represented by predominantly single arcs, as in cases of polycrystalline ionic conductors without blocking grain boundaries [34, 38]. Characterization at low frequencies is missing. HPNT electrical conductivity in wet atmospheres was an order of magnitude lower, as expected from its lesser content in niobium, and therefore less acid nature.

The electrical conductivity of HPN exhibited a minimum when heated to higher temperatures (Fig. 10). This has been observed in other H-based pyrochlores [7, 9]. The data from Guo et al. [9] are shown in Fig. 10, for comparison to ours. The initial decrease in electrical conductivity is explained by water loss at surfaces and grain boundaries. Above 130 °C, the conductivity increased, which we attribute to translocation of protons between water near oxygen vacancy sites, protonated water diffusing in internal channels [3, 26] and/or proton translocation between hydroxyl groups. HPN conductivity decreased when the material became amorphous. HPN activation energy at the higher temperatures was 0.2 eV, which is within the range (0.2 eV–0.4 eV) typical of polycrystalline fast (superionic) conductors [3, 26], suggesting that high conductivities could be achieved by repressing thermal decomposition.

The rise in the electrical conductivity, when switching from dry to wet atmospheres (Fig. 11), is attributed to water uptake at surfaces. The conductivity samples consisted of cold pressed HPN powders that had been dried at 130 °C, consistent with the formula $H_{2.66}Pb_{0.17}Nb_2O_{6.5}{\cdot}0.5H_2O$. No significant water uptake should have taken place at the oxygen vacancy sites (1/2 of 8b sites) of the non-stoichiometric pyrochlore, which were already filled with water. Consistently, HPN conductivity in a dry atmosphere was comparable to the "intrinsic" (intra-crystalline) conductivity of defective pyrochlores, estimated from their NMR data by Butler and Biefeld [18].

The rise in HPN conductivity with time (Fig. 11) can be interpreted in terms of a diffusion–adsorption model: Water

vapor adsorbs quickly at external surfaces followed by a slower step, to diffuse into the inter-particle spaces of the compacted powders. Thus, the change in electrical conductivity with time measures the rate of water uptake by HPN.

The kinetics of diffusion in porous materials followed by fast adsorption at the pore walls has been analyzed in the literature [39–41]. Solutions to the Fick equations provide expressions for interpreting experimental results (Fig. 11). The conductivity samples are approximated by spheres of the same volume. With the mean concentration (C) of water in the sample being C_0 at time zero, and C_2 at time infinite, the normalized concentration-time profile in a sphere of radius r, is [40]:

$$(C - C_2)/(C_0 - C_2) = (6/\pi^2) \sum_{n=0}^{\infty} \left(\frac{1}{n^2}\right) \exp\left[\frac{-n^2\pi^2 Dt}{r^2}\right] \tag{1}$$

Considering only the first term in the series and applying logarithms, the approximate solution, for a sphere of radius $r = 0.26$ cm, is:

$$\begin{aligned} \ln\left[(C - C_2)/(C_0 - C_2)\right] &= \ln(6/\pi^2) \exp\left[(-\pi^2 D\, t)/r^2\right] \\ &= -0.4977 - 146.0\, D\, t \end{aligned} \tag{2}$$

Rearranging terms, and replacing concentration with electrical conductivity:

$$\begin{aligned} \ln(\sigma_{\text{infinite}} - \sigma) &= \ln(\sigma_{\text{infinite}} - \sigma_0) - 0.497 - 146.0\, D\, t \\ &= \text{constant} + t/\tau \end{aligned} \tag{3}$$

The experimental data of Fig. 11 were fit to Eq. 3, with a fitting parameter of $\sigma_{\text{infinite}} = 1.65 \times 10^{-5}$ S cm^{-1}. Figure 12 shows the quality of fit. The conductivity reached 63% of its final value at a characteristic time $\tau = 10$ h. The associated diffusion coefficient was 1.9×10^{-7} cm^2/s. This represents an effective coefficient for the diffusion of water vapor in the porous compact. Its value falls within the range of values reported for other porous materials at room temperature. For example, the diffusion coefficients of water in polymers are between 10^{-4} and 10^{-12} cm^2/s [42, 43] and in fibrous paper 10^{-7} cm^2/s [44]. In a sintered ceramic (BCN18), the chemical diffusion coefficient of water was reported to be approximately 2.5×10^{-6} cm^2/s, at 700 °C [45].

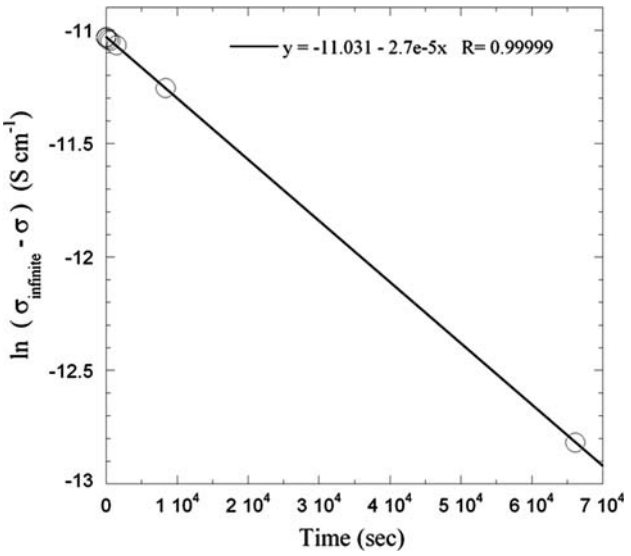

Fig. 12 Fit with Eq. 3 to the conductivity data in Fig. 11, plotted versus time, after subtraction from $\sigma_{\text{infinite}} = 1.65 \times 10^{-5}$ S cm^{-1}

Conclusions

Two new compounds, HPN and HPNT, in the form of white powders of sub-micron particle size, were obtained by cation exchange in PN and PNT, heated in aqueous solutions of nitric and hydrochloric acids. The crystalline pyrochlore framework was conserved after the exchange. The new pyrochlores contained small quantities of residual lead.

Both HPN and HPNT lost weight upon heating, due to H_2O being released. Only weight changes in HPN were reversible and the structure preserved, independently of the gas atmosphere (He, O_2, or N_2), when the powder samples were heated to and kept at 170 °C for 2 h, and then cooled down. The weight re-gained is attributed to absorbed water, originally in the cylinders of carrier gases. At above 250 °C, the pyrochlore structure collapsed in both, HPN and HPNT, yielding amorphous products and at higher temperatures, crystalline phases of smaller particle size.

The effective formulas derived from chemical analyses, and corroborated by TGA data, were $H_{2.66}Pb_{0.17}Nb_2O_{6.5}{\cdot}0.5\ H_2O$ (HPN) and $H_{3.88}Pb_{0.06}Nb_{1.33}Ti_{0.67}O_{6.67}{\cdot}0.33\ H_2O$ (HPNT). They led to successful Rietveld refinements, which confirmed the preservation of the pyrochlore structure. Densities measured by pycnometry were in agreement with densities evaluated from the refined lattice parameters and the effective formulas.

Moderate electrical conductivities were measured in wet atmospheres: 10^{-6} to 10^{-5} S cm^{-1} for HPN, and 10^{-7} to 10^{-6} S cm^{-1} for HPNT, at temperatures between room and 230 °C. The conductivity was higher in HPN than in HPNT by an order of magnitude, attributable to HPN being richer in Nb(V), which strongly interacted with adsorbed water molecules, releasing protons for conduction. HPN electrical conductivity increased when switching from a dry to a wet atmosphere; the data were interpreted by a diffusion/adsorption model.

Acknowledgements The authors gratefully acknowledge Dr. Shuling Guo and Dr. J.-P. Belieres for obtaining DSC data, Dr. Z. Liu for taking SEM micrographs, Dr. K. Leinenweber and F. He for helping with XRD, and Barry Wilkens for performing the Ion Beam Analysis. Financial support from the Air Force Office of Scientific Research under grants 155A-99-0031 and FA95500410153 is also gratefully acknowledged.

Appendix: Analysis of residual lead by anodic stripping voltammetry

This electrochemical method was selected to determine residual lead in HPN and HPNT, because of its simplicity and adequacy to the type of samples investigated. The procedure developed was based on fundamentals and applications given in the literature [46, 47].

Lead in HPN

HPN powders dried at 130 °C and in the amount of 260 mg/100 mL, were dissolved in a 3:2 mixture of HNO_3 (1:1) and H_2O_2 (30%), at 60–70 °C, with magnetic stirring, for several hours. Stripping analysis was carried out in a three electrode EG&G glass cell and with an EG&G Princeton applied research potentiostat/galvanostat Model 263 A, operated by Power Suite software. Recorded data were graphed with Kaleidagraph software. The electrodes included a silver/silver chloride/KCl 4 M reference electrode with a porous frit glass junction, a glassy carbon (2.5 mm diameter) working electrode, and a platinum wire counter electrode. The cell and the Pt electrode were cleaned with 10% v/v HNO_3. The glassy carbon electrode was cleaned with silicon carbide paper and with alumina.

The voltage/time program applied to the electrochemical cell consisted of a constant potential step a –0.7 V (to reduce lead and the mercury film) followed by a linear stripping scan between –0.7 and 0 V, at 100 mV/s (to oxidize the lead). The deposition at –0.7 V was done for 60 s under bubbling nitrogen, followed by 15 s equilibration at the same potential, and then a linear scan, both under still conditions. Reagents and solutions utilized were: reagent grade Baker KNO_3, nanopure water, reagent grade Fischer Scientific $Hg(NO_3)_2{\cdot}H_2O$ in a 2×10^{-2} M aqueous solution (pH 1), standard Pb(II) solution (VHG, 1,000 μg/mL), and standardized $Pb(NO_3)_2$ solution (2 mM nominal).

Control experiments were run in a 10 mL solution of 0.1 M KNO_3 and 5.0×10^{-2} M $Hg(NO_3)_2$ in nanopure water, after bubbling nitrogen for 20 min. No peaks were detected in the control experiments. A measured volume (15 μL) of the solution with dissolved HPN was added to the cell. After adequate purging, the voltage/time program was applied. A small peak at about –0.32 V was observed. This measurement was repeated. Afterwards, the solution in the stripping cell was "spiked" with three successive additions of a lead solution of known concentration (standard addition method). Two runs were recorded after each addition. The data were plotted as current/voltage. The areas under the stripping peaks were integrated, between adequate limits. After subtraction of the background, the areas were converted to charges and graphed versus the lead concentration due to spiking (standard additions). The graphs consisted of straight lines (one for each analysis) of different slopes. The difference in slopes was caused by different hydro-dynamical conditions. When extrapolated to charge zero, the lines intercepted the abscissa at a common concentration value. This extrapolated concentration corresponded to the lead content before spiking, which is the lead from dissolved HPN. Peak currents were also graphed as a function of lead concentration, but the corresponding extrapolated concentration values were less reproducible than in the case of graphing integrated areas versus lead concentration.

Lead in HPNT

The same procedure described to determine lead in HPN was followed for HPNT. The amount of HPNT dissolved in the acid solution was 300 mg/100 mL.

References

1. Mangham RI (2003) Ph.D. Dissertation, Arizona State University
2. Groult D, Michel C, Raveau B (1974) Inorg Nucl Chem 36:61
3. England WA, Cross MG, Hamnett A, Wiseman PJ, Goodenough JB (1980) Solid State Ionics 1:231
4. Chowdhry U, Barkley JR, English AD, Sleight AW (1982) Mat Res Bull 17:917
5. Turrillas X, Delabouglise G, Jouberet JG, Fournier T, Muller J (1985) Solid State Ionics 17:169
6. Clearfield A (1988) Chem Rev 88:125
7. Catti M, Mari CM, Cazzanelli E, Mariotto G (1990) Solid State Ionics 40/41:900
8. Lewandowski JT, Pickering IJ, Jacobson AJ (1992) Mat Res Bull 27:981
9. Guo J-D, Reis KP, Whittingham MS (1992) Solid State Ionics 53–56:305
10. Möller T, Clearfield A, Harjula R (2001) Chem Mater 13:4767
11. Aleshin E, Roy R (1962) J Am Chem Soc 45:18
12. Subramanian MA, Aravamudan G, Subba Rao GV (1983) Prog Solid State Ch 15:55
13. Sleight AW (1968) Inorg Chem 7:1704
14. Wilde PJ, Catlow CRA (1968) Solid State Ionics 112:173
15. Sickafus KE, Minervini L, Grimes RW, Valdez JA, Ishimaru M, Li F, McClellan KJ, Hartmann T (2000) Science 229:748
16. Hahn T (ed) (2002) International tables of crystallography, Vol A. Kluwer Academic Publisher, Dordrecht, p 696
17. Vanderborne MT, Husson E (1984) J Solid State Chem 53:253
18. Butler MA, Biefeld RM (1979) Phys Rev B 19:5455
19. England WA, Slade RCT (1980) Solid State Commun 33:997

20. Groult D, Pannetier J, Raveau B (1982) J Solid State Chem 41:277
21. Dickens PC, Weller MT (1986) Solid State Commun 59:569
22. Doremieux-Morin C, Fraissard JP, Besse JP, Chevalier R (1985) Solid State Ionics 17:93
23. Slade RCT, Hall GP, Ramanan A, Prince E (1996) Solid State Ionics 92:171
24. Alonso JA, Turrillas X (2005) Dalton Trans (5):865
25. Trubnikov IL (2000) Refract Ind Ceram 41:396
26. Colomban P (1992) Proton conductors. Cambridge University Press, Cambridge, p 284
27. Wachs JE, Jehng JM, Deo G, Hu H, Arora N (1996) Catal Today 28:199
28. Zuo Z, Ye J, Arakawa H (2003) Int J Hydrogen Energ 28:663
29. Lucas P, Petuskey WT (2001) J Am Ceram Soc 84:2150
30. Mangham R, Petuskey WT (2005) Ceram Trans 169:139
31. Remy H (1956) Treatise on inorganic chemistry, vol II. Elsevier, Amsterdam, p 108
32. Larson AC, Von Dreele RB (1994) General Structure Analytic System (GSAS), Los Alamos National Laboratory Report (LAUR 86–748 (1994))
33. Beech F, Jordan WM, Catlow CRA, Santoro A, Steele BCH (1988) J Solid State Chem 77:322
34. Bauerle JE (1969) J Phys Chem Solids 30:2657
35. Traversa E (1985) Sensor Actuat B 223:135
36. Larring Y, Norby T (1997) Solid State Ionics 97:523
37. Colomban P, Romain F, Neiman A, Animitsa I (2001) Solid State Ionics 145:339
38. Brune A, Wagner JB Jr. (1995) Mater Res Bull 30:573
39. Crank J (1952) Philos Mag 43:811
40. Ruthven DM (1984) Principles of adsorption and adsorption processes. J. Wiley, New York, p 168
41. Glicksman ME (2000) Diffusion in solids: field theory, solid state and applications. J. Wiley, New York, p 101
42. Barrie JA (1968) In: Crank J, Park GS (eds) Diffusion in polymers. Academic Press, London, p 276
43. Fukuda M (1996) Polym Eng Sci 36:558
44. Yoon S-H, Jeon Y (1998) Palpu Chongi Gisul 30:46
45. Wang W, Virkar AV (2004) Sensor Actuat B 98:282
46. Brainina KH, Neyman E (1993) Electroanalytical stripping methods. John Wiley, New York, p 5
47. Wang J (1985) Stripping analysis. VCH, New York, p 32